Neuron, Vol. 44, 453–467, October 28, 2004, Copyright ©2004 by Cell Press

# Quaternary Structure, Protein Dynamics, and Synaptic Function of SAP97 Controlled by L27 Domain Interactions

**Terunaga Nakagawa,[1,2,3,7] Kensuke Futai,[1,2,4,7] Hilal A. Lashuel,[5] Irene Lo,[1] Kenichi Okamoto,[1,2] Thomas Walz,[6] Yasunori Hayashi,[1,2,*] and Morgan Sheng[1,2,3,*]**

[1]The Picower Center for Learning and Memory
[2]RIKEN-MIT Neuroscience Research Center
[3]Howard Hughes Medical Institute
Massachusetts Institute of Technology
77 Massachusetts Avenue
Cambridge, Massachusetts 02139
[4]Laboratory for Neural Architecture
Brain Science Institute
RIKEN
Wako, Saitama 351-0198
Japan
[5]Center for Neurologic Diseases
Brigham and Women's Hospital and
Department of Neurology
Harvard Medical School
65 Lansdowne Street
Cambridge, Massachusetts 02139
[6]Department of Cell Biology
Harvard Medical School
240 Longwood Avenue
Boston, Massachusetts 02115

## Summary

**Single-particle electron microscopy (EM) combined with biochemical measurements revealed the molecular shape of SAP97 and a monomer-dimer transition that depended on the N-terminal L27 domain. Overexpression of SAP97 drove GluR1 to synapses, potentiated AMPA receptor (AMPAR) excitatory postsynaptic currents (EPSCs), and occluded LTP. Synaptic potentiation and GluR1 delivery were dissociable by L27 domain mutants that inhibit multimerization of SAP97. Loss of potentiation was correlated with faster turnover of monomeric SAP97 mutants in dendritic spines. We propose that L27-mediated interactions of SAP97 with itself or other proteins regulate the synaptic delivery of AMPARs. RNAi knockdown of endogenous PSD-95 depleted surface GluR1 and impaired AMPA EPSCs. In contrast, RNAi knockdown of endogenous SAP97 reduced surface expression of both GluR1 and GluR2 and inhibited both AMPA and NMDA EPSCs. Thus SAP97 has a broader role than its close relative, PSD-95, in the maintenance of synaptic function.**

## Introduction

In excitatory synapses of the brain, the neurotransmitter glutamate released from the presynaptic terminal activates glutamate receptors present at high density in the postsynaptic density (PSD). The PSD contains numerous cytoskeletal and signaling proteins that are held together by a set of scaffold proteins, among which the PSD-95 (also known as SAP90) family of membrane-associated guanylate kinase (MAGUK) proteins is prominent (Cho et al., 1992; Husi et al., 2000; Kistner et al., 1993; Peng et al., 2004; Walikonis et al., 2000).

PSD-95 family proteins share a common domain organization, consisting of three PDZ domains followed by an SH3 domain and a C-terminal guanylate kinase-like (GK) domain (Figure 1A). These domains serve as modular sites for protein-protein interactions and are highly conserved in sequence and binding specificity between different members of the PSD-95 family. By binding to NMDA receptors (NMDARs) and a variety of cytoplasmic signaling molecules, PSD-95 family proteins are believed to direct the downstream signaling pathways activated by NMDARs, thereby mediating postsynaptic plasticity mechanisms (Husi et al., 2000; Migaud et al., 1998; Sheng and Kim, 2002).

The atypical member of the PSD-95 family is SAP97 (also known as hDlg). In contrast to its three close relatives (PSD-95, PSD-93/chapsyn-110, and SAP102), SAP97 is not specifically associated with NMDARs in brain and is not highly enriched in the PSD (Kim et al., 1996). Instead, SAP97 is associated more with light membrane fractions and cytosol and interacts specifically with AMPARs (Leonard et al., 1998; Sans et al., 2001). The C-terminal tail of the AMPAR subunit GluR1 has been reported to bind directly to the PDZ domains of SAP97 (Cai et al., 2002; Leonard et al., 1998). This finding is puzzling because, based on the high conservation of amino acid sequences (see Figure 1A), the PDZ and other domains of SAP97 should have binding specificities similar to those of PSD-95 (Hung and Sheng, 2002; Songyang et al., 1997). Indeed, according to both in vitro and yeast two-hybrid assays, the PDZ domains of SAP97 bind to the C termini of NR2A and NR2B indistinguishably from PSD-95 and PSD-93 (Bassand et al., 1999; Niethammer et al., 1996). So why does SAP97 behave so differently from PSD-95 in vivo?

To understand the structural basis of their functional differences, we investigated the molecular anatomy of the full-length PSD-95 and SAP97 proteins with single-particle EM combined with biophysical analysis. The overall shapes of these two scaffolds are strikingly different in the monomeric state. In addition, SAP97 shows a propensity for multimerization via its N-terminal L27 domain. Analysis of multimerization mutants in neurons shows that L27-mediated interaction is important for the protein dynamics and synaptic function of SAP97.

It is well established that PSD-95 potentiates synaptic transmission, at least in part, by mediating the recruitment of AMPARs (Ehrlich and Malinow, 2004; El-Husseini et al., 2000; Schnell et al., 2002; Stein et al., 2003). In comparison, the role of SAP97 in AMPAR trafficking and synaptic function is controversial (Hayashi et al., 2000; Rumbaugh et al., 2003; Schnell et al., 2002). Here we report that overexpression of SAP97 potentiates synaptic transmission and drives GluR1 AMPARs to synapses. Interestingly, these two effects can be dissoci-

*Correspondence: msheng@mit.edu (M.S.); yhayashi@mit.edu (Y.H.)
[7]These authors contributed equally to this work.

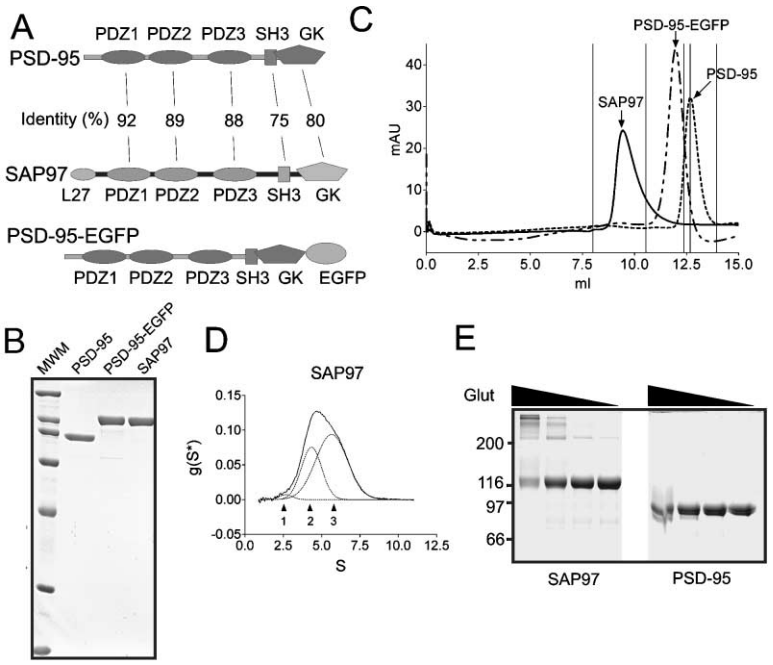


Figure 1. Biochemical Characterization of Purified PSD-95 and SAP97

(A) Domain organization of PSD-95 and SAP97. Numbers indicate percent identity between individual domains.

(B) Coomassie blue-stained SDS-PAGE of purified PSD-95, PSD-95-EGFP, and SAP97. The molecular weight marker (MWM) in kDa (200, 116, 97, 66, 45, 31, 21.5).

(C) Analytical gel filtration of recombinant proteins in (B). Thin vertical lines indicate the position of molecular weight/Stokes' radius standards (from left, Blue Dextran 2000 = void; ferritin = 61.0 Å; catalase = 52.2 Å; aldolase = 48.1 Å; BSA = 35.5 Å). Horizontal axis indicates the Ve (in ml). Vertical axis shows absorbance at 280 nm.

(D) Analytical ultracentrifugation of SAP97. The distribution of sedimentation coefficients (Svedberg units) of purified SAP97 is shown as a solid line. The data distribution can be deconvoluted into three Gaussian distributions (dotted lines, peak positions labeled 1–3, of which 2 + 3 are major).

(E) Chemical crosslinking of SAP97 by glutaraldehyde. Purified SAP97 and PSD-95 in solution (0.1 mg/ml) were individually treated with increasing concentrations (0.0006%, 0.002%, 0.006%, 0.02%) of glutaraldehyde and subjected to SDS-PAGE and Coomassie blue staining.

ated, with the former, but not the latter, dependent on multimerization of SAP97 via its L27 domain. The importance of SAP97 for synaptic transmission and surface expression of AMPARs was confirmed by RNA interference (RNAi) experiments that revealed unexpected differences between the functions of SAP97 and PSD-95.

## Results

### Biophysical Characteristics of PSD-95 and SAP97

PSD-95, PSD-95-EGFP, and SAP97 (all hexahistidine-tagged) were expressed in Sf9 cells as recombinant proteins and purified. The resulting proteins ran as single bands at the expected molecular weight (MW) and were >95% pure (Figure 1B). To derive the native MW of the particles in solution, the Stokes radius and sedimentation coefficient (S) of the highly purified soluble proteins were determined by analytical gel filtration and analytical ultracentrifugation (see Experimental Procedures and Table 1). The native MW of PSD-95 was estimated to be 67 kDa, which is in keeping with a monomeric particle of globular shape (MW = 81 kDa) (Table 1). In contrast, SAP97 has a native MW of 131 kDa, a value between the MW of a monomer (97 kDa) and that of a dimer (194 kDa). This suggests either an asymmetric shape or the presence of multimeric forms of SAP97 in solution.

In analytical gel filtration, elution volume (Ve) of SAP97 was smaller than PSD-95, indicating a larger molecular size for SAP97 (Figure 1C). However, the difference in Ve was greater than predicted from the different MW of these two proteins. This is highlighted by the fact that SAP97 elutes faster than PSD-95-EGFP (Figure 1C), which migrates to about the same position as SAP97 on SDS-PAGE (Figures 1B and 1C). The discrepancy suggests that SAP97 forms multimers or has a highly asymmetric shape.

The elution profile of PSD-95 from the gel filtration column showed a narrow symmetric Gaussian distribution. SAP97, however, eluted in a broader asymmetric peak, suggestive of a heterogeneous population of particles (Figure 1C). When deconvoluted into multiple Gaussian curves, the distribution of S values of SAP97 could be accounted for by the presence of two major species (Figure 1D). In contrast, PSD-95 exhibited a "monophasic" distribution (see Figure 3E). Taken together, we conclude that purified SAP97 likely exists in an equilibrium between monomer and dimer in solution, whereas PSD-95 exists predominantly in monomeric form. However, these biophysical measurements do not

Table 1. Size Measurements of PSD-95 and SAP97 Particles

| Protein | Stokes' Radius (Å) | Sedimentation Coefficient (S) | Native Molecular Weight (kDa) | Molecular Weight (kDa) |
|---|---|---|---|---|
| PSD-95 | 46.5 | 3.5 | 67 | 81 |
| SAP97 | 72.9 | 4.4 | 131 | 97 |
| ΔL27 SAP97 | 53.6 | 3 | 66 | 93 |
| I38G-SAP97 | 56 | 3.4 | 78 | 97 |

exclude the possibility of a dynamic conformational equilibrium.

To confirm the presence of a multimerized population of SAP97, we performed a chemical crosslinking assay (Figure 1E). Purified PSD-95 and SAP97 in solution were incubated with the crosslinking agent glutaraldehyde and then separated by SDS-PAGE. Glutaraldehyde caused the appearance of a SAP97 band at ~220 kDa (presumptive dimer) as well as slower migrating species with higher concentrations of the crosslinking agent (Figure 1E). Under the same conditions, purified PSD-95 formed no dimer/multimer species. Thus, SAP97 self-associates whereas PSD-95 remains monomeric in solution.

### Molecular Structures of PSD-95 and SAP97 by EM

To determine directly the size and shape of SAP97 and PSD-95, we used negative-stain EM combined with digital image processing to visualize individual molecules of the purified proteins. Particles from digitized electron micrographs (~3000 particles for PSD-95 and ~12,000 particles for SAP97) were analyzed by multivariate statistical analysis, image classification, and multireference alignment. PSD-95 particles were relatively homogeneous in size and shape (~100 Å in length and 60 Å in width), and the majority existed in a C-shaped or "horseshoe" conformation, consistent with an extended molecule that is curled back on itself (Figures 2A and 2E). We speculate that the open ends of the "C" correspond to the N and C termini of PSD-95 protein. In some cases, PSD-95 particles had a doughnut shape in which no break in the ring was obvious (Figure 2A).

SAP97 particles were more heterogeneous. The majority (~65% of "monomeric" particles) appeared as extended rod-like structures (~150 Å in length) (Figure 2B). The remainder (~35%) had a C-shaped or ring-like structure similar to that of PSD-95 (Figure 2C). It is striking that the averages of the monomeric form of SAP97 resolved four clearly separable globules, especially in the extended configuration (Figures 2B and 2E). The linear array of globules probably represents the linked domains of SAP97, though more work is required to identify their submolecular nature.

In addition to the monomeric particles of SAP97, we detected many larger particles (Figure 2D), which were absent in PSD-95 preparations, that likely represent dimers. These EM findings are consistent with the monomer-dimer equilibrium of SAP97, which is inferred from gel filtration (Figure 1). The individual molecules were not well resolved in the class averages of dimeric SAP97 due to structural heterogeneity in the particles, suggesting considerable flexibility of the dimeric structure. This is not surprising considering the degree of flexibility observed in the class averages of monomeric PSD-95 and SAP97. In the various averaged images of PSD-95, the two ends of the molecule were positioned at slightly different distances relative to each other. In the extended monomers of SAP97, the rods showed bends and kinks of varying angles among the various classes. In summary, the differential hydrodynamic properties of PSD-95 and SAP97 can be accounted for by the compact shape of PSD-95 monomers versus the more extended configuration and multimerization of SAP97.

### Multimerization of SAP97 by L27 Domain

What is the molecular basis for the self-association of SAP97? The N-terminal region of SAP97 contains an L27 domain (65 amino acids), which has been implicated in heterodimerization between Lin-2 and Lin-7 in *C. elegans* (Doerks et al., 2000). In GST pull-down assays, a GST-fusion of the L27 domain of SAP97 precipitated wild-type full-length SAP97 but not a deletion mutant lacking the L27 domain (ΔL27SAP97; Figure 3B). Moreover, the ΔL27SAP97 mutant showed a large reduction in particle size as judged by analytical gel filtration and native MW, consistent with its being a monomer (Figure 3C; Table 1). These results demonstrate that the L27 domain is necessary and sufficient for SAP97 multimerization.

To identify L27 mutants that affect SAP97 multimerization, 23 single amino acid substitutions of full-length SAP97 were expressed, purified, and screened by analytical gel filtration (Figure 3D). Mutations were identified that increase (L14G, L15G, E26A, D27A, and Q42A) or decrease the Stokes' radius (I34G, V37G, I38G, and F41A), implying increased or decreased multimerization, respectively (Figures 3C, 3D, and 3G). Interestingly, these residues are among the most conserved in known L27 domains (see boxes in Figure 3A). We focused on I38G and L14G as representative mutants in the following experiments. I38G sediments similarly to PSD-95 and more slowly than wild-type SAP97, consistent with I38G-SAP97 being a monomer (Figures 3E and 3F). SDS-PAGE revealed no difference in the mobility of wild-type, I38G mutant, and L14G mutant SAP97 (Figure 3H). In native PAGE, however, I38G migrated faster than did wild-type, while the L14G mutant migrated more slowly (Figure 3I). These results are consistent with I38G-SAP97 existing primarily in the monomeric state, while wild-type and L14G-SAP97 exist in monomer-dimer equilibria, with L14G shifted more toward dimer than wild-type. Finally, we confirmed by chemical crosslinking experiments that the I38G mutant is monomeric. When equal amounts of purified SAP97 variants in solution were treated with increasing concentrations of glutaraldehyde, dimeric (and higher) species were observed only for wild-type and L14G (Figure 3J).

### Homomultimerization of SAP97 Detected in Neurons

Next we used fluorescence resonance energy transfer (FRET) to determine if SAP97 also forms homomultimers in neurons. Because SAP97 self-associates via its L27 domain, we monitored multimerization in live neurons as a function of FRET efficiency (E) between N-terminally tagged CFP-SAP97 and YFP-SAP97 (Supplemental Figure S1 [http://www.neuron.org/cgi/content/full/44/3/453/DC1/]). To reduce pH dependence, the Venus variant of YFP was used (Nagai et al., 2002).

In dissociated hippocampal neurons (DIV16-17), CFP- and YFP-SAP97 were both enriched at steady state in dendritic spines 1 to 2 days after transfection (in agreement with a previous report [Rumbaugh et al., 2003], our SAP97 constructs also included the I3 insert).

When CFP-SAP97 and YFP-SAP97 were coexpressed in neurons, we detected FRET in dendritic spines ($E = 0.074 \pm 0.019$) (Supplemental Figure S1 [http://www.

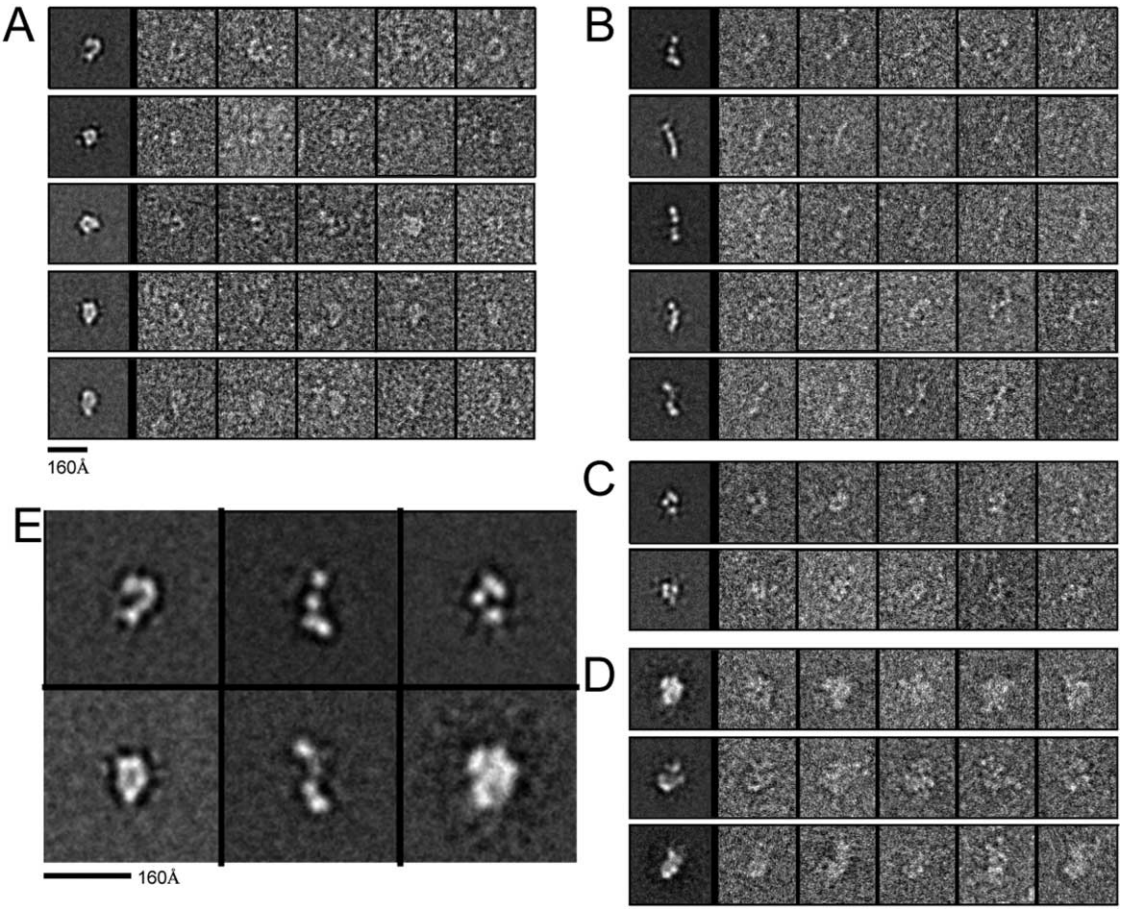


Figure 2. EM Images of PSD-95 and SAP97

Each row shows the class average (left) and five representative raw images contained in the corresponding class average (right). (A) PSD-95 particles. (B) Monomers of SAP97 in an extended conformation. (C) Monomers of SAP97 in a compact conformation. (D) Multimeric SAP97. (E) Enlarged representative class averages of PSD-95 (left panels), extended monomeric SAP97 (middle panels), closed monomeric SAP97 (right top panel), and multimeric SAP97 (right bottom panel). Scale bars, 160 Å.

neuron.org/cgi/content/full/44/3/453/DC1/]). The monomeric I38G mutant was also enriched in spines (see Figure 6A), but the level of FRET between CFP-I38G-SAP97 and YFP-I38G-SAP97 in neurons was significantly smaller ($E = 0.017 \pm 0.016$) (Supplemental Figure S1). These results indicate that SAP97 can homomultimerize via its L27 domain in dendritic spines of living neurons, but they do not exclude L27-mediated heteromultimerization of SAP97 with other proteins.

### Effects of SAP97 Overexpression on Synaptic Transmission

Based on GST pull-down assays, the isolated wild-type L27 domain can interact with wild-type SAP97, I38G-SAP97, and L14G-SAP97 (Figure 3B). However, more quantitative biophysical analysis definitively shows that I38G-SAP97 is predominantly monomeric and L14G-SAP97 is mainly dimeric in solution, with wild-type SAP97 being intermediate (Figure 3, Table 1). We compared the effects of overexpression of these SAP97 variants in CA1 neurons of hippocampal organotypic slice cultures (Figure 4). Since GFP tagging might affect SAP97 structure-function, we used SAP97 constructs without epitope tags. Simultaneous recordings were obtained from both transfected neurons (identified by cotransfection with GFP) and a neighboring untransfected neuron in response to stimulation of Schäffer collateral fibers. Neurons overexpressing wild-type SAP97 showed a robust increase in amplitude of AMPAR EPSCs compared with untransfected cells (187.8% $\pm$ 27.4%), along with a slight and insignificant reduction in the NMDAR EPSCs, resulting in an elevated AMPA/NMDA ratio (Figures 4B, 4E, and 4F). L14G-SAP97 caused a similarly large increase in AMPAR EPSCs with no change in NMDAR EPSCs (Figures 4C, 4E, and 4F). In contrast, the I38G mutant slightly suppressed both AMPAR and NMDAR currents (Figures 4A and 4E). Overexpression of PSD-95 in hippocampal slice cultures strongly enhanced AMPAR EPSCs with little effect on NMDAR EPSCs (Figure 4D), as previously reported (Ehrlich and Malinow, 2004; Schnell et al., 2002; Stein et al., 2003).

We also measured the quantal events of synaptic response in neurons overexpressing different SAP97 mutants by recording asynchronous miniature EPSCs in the presence of $Sr^{2+}$ (Supplemental Figure S2 [http://www.neuron.org/cgi/content/full/44/3/453/DC1/]) (Sala et al., 2003). Quantal size was significantly reduced in

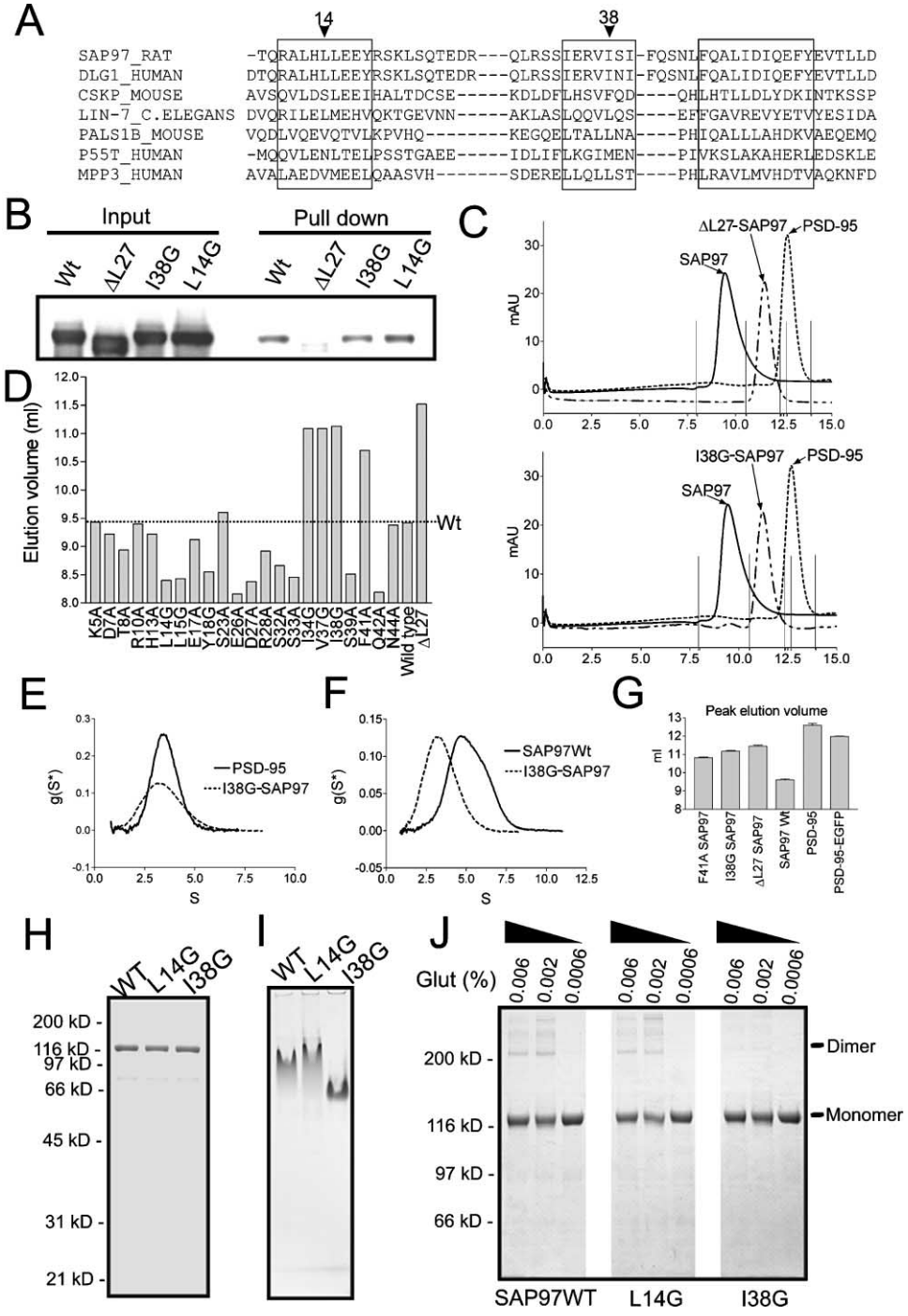


Figure 3. Biochemical Characterization of SAP97 Mutants

(A) Aligned sequence (ClustalW) of the L27 domain from different proteins in the SWISS-PROT database. Highly conserved residues are boxed; L14 and I38 are indicated.

(B) GST pull-down of wild-type and mutant SAP97 proteins by GST-fusion of SAP97 L27 domain. Precipitated proteins were immunoblotted with anti-SAP97 antibody.

(C) Analytical gel filtration of ΔL27-SAP97 and I38G-SAP97 compared with wild-type SAP97 and PSD-95. Solid vertical lines indicate Stokes' radius standards as in Figure 1C.

(D) Peak elution volume of L27 domain mutants of SAP97 measured by analytical gel filtration, compared with wild-type SAP97 (horizontal dotted line).

(E and F) Analytical ultracentrifugation comparing I38G-SAP97 with wild-type SAP97 and PSD-95.

(G) Peak elution volume of purified wild-type and mutant SAP97 compared with PSD-95 and PSD-95-EGFP.

(H) SDS-PAGE of purified wild-type and L14G and I38G mutants of SAP97.

(I) Native-PAGE of purified wild-type, L14G-, and I38G-SAP97.

(J) Chemical crosslinking of purified proteins by glutaraldehyde (Glut). Purified wild-type SAP97, I38G-SAP97, and L14G-SAP97 in solution (0.1 mg/ml) were treated with increasing concentrations of glutaraldehyde (percent weight/volume) and subjected to SDS-PAGE and Coomassie blue staining.

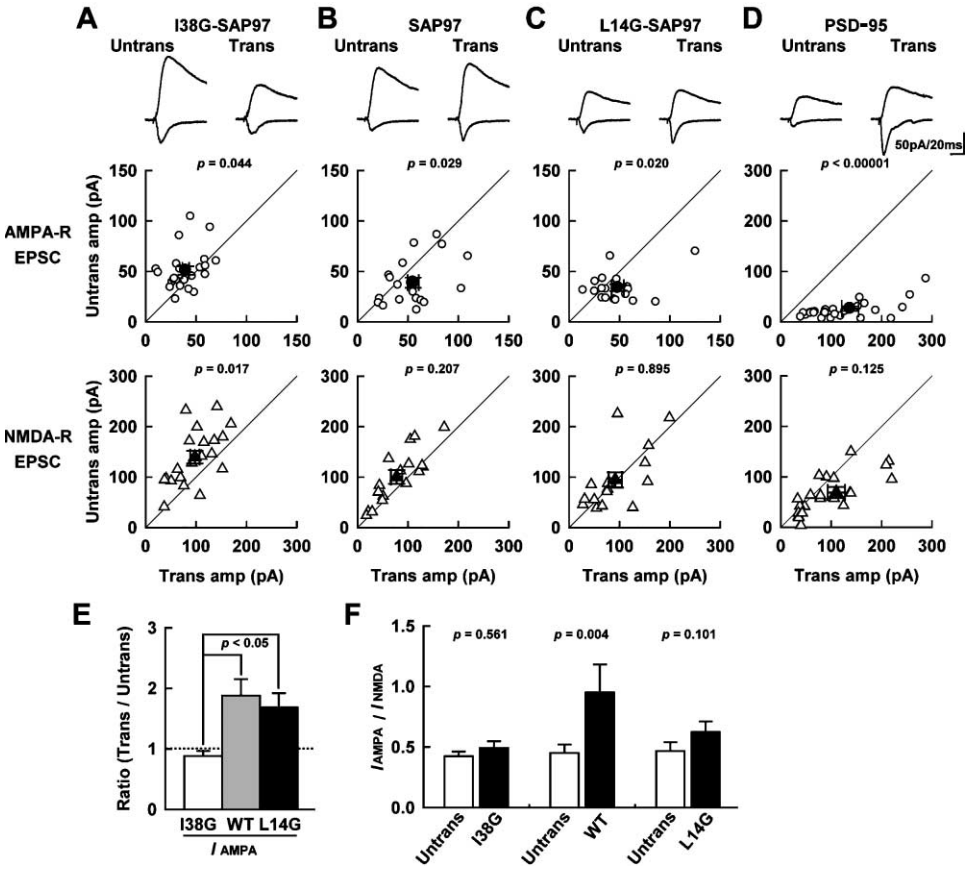


Figure 4. Effect of Wild-Type and L27 Domain Mutants of SAP97 on Synaptic Transmission

(A–D) Sample EPSC traces mediated by AMPAR (downward) and NMDAR (upward) from pairs of transfected (Trans) and neighboring untransfected (Untrans) cells (top). EPSC amplitudes (AMPAR EPSCs [middle] and NMDAR EPSCs [bottom]) were plotted for each pair of transfected and neighboring untransfected cells. Open symbols represent single pairs of recordings. Filled circles indicate the mean ± SEM. (A) I38G-SAP97 mutant. (B) Wild-type SAP97. (C) L14G-SAP97 mutant. (D) PSD-95. Numbers of cell pairs were I38G (AMPAR-EPSCs/NMDAR EPSCs: 23/20); SAP97 wild-type (20/16); L14G (18/16); PSD-95 (18/15).

(E) Summary of effect of SAP97 constructs on AMPAR EPSCs. Each bar represents average of ratios obtained from multiple pairs of transfected and untransfected neighboring neurons. $p < 0.05$ (Kruskal-Wallis ANOVA).

(F) Summary of AMPAR EPSC/NMDAR EPSC ratios in neurons transfected with SAP97 variants versus untransfected neighboring cells.

I38G-SAP97-expressing cells and enhanced in L14G-SAP97-expressing cells (Supplemental Figures S2A3–S2B3). The frequency of events was reduced by I38G and enhanced by L14G (Supplemental Figures S2A4–S2B4). However, paired-pulse facilitation was not significantly altered by overexpression of SAP97 or its mutants (Supplemental Figure S2C). These results argue against any effect on presynaptic release probability but are consistent with postsynaptic action of SAP97 on AMPARs. Overall, we conclude that SAP97, like PSD-95, selectively enhances AMPAR EPSCs. Notably, this potentiating effect requires a functional L27 domain.

### SAP97 Delivers GluR1 to the Synapse

Because SAP97 and GluR1 interact with each other, we asked if SAP97 can drive GluR1 to the synapse. Overexpressed GluR1 tends to form homomeric inwardly rectifying channels; thus synaptic incorporation of GluR1 receptors can be monitored by measuring the rectification index (RI; ratio of AMPAR EPSCs at −60 and +40 mV) (Figure 5) (Hayashi et al., 2000). Transfection of GluR1 had no effect on mean EPSC amplitudes (untransfected: 50.4 ± 3.7 pA; transfected: 45.4 ± 3.0 pA; $p = 0.41$, $n = 19$ cell pairs) or RI (untransfected: 2.52 ± 0.11; transfected: 2.89 ± 0.23; $p = 0.60$, $n = 18$ cell pairs), indicating no synaptic delivery of GluR1 receptors by overexpression of GluR1. Overexpression of SAP97 constructs in the absence of GluR1 had no effect on RI (Figures 5A4–5C4, left). A significant increase in RI was observed, however, when wild-type or I38G or L14G mutants were coexpressed with GluR1 (Figures 5A4–5C4, right). Concomitant increases in EPSC amplitude with wild-type and L14G-SAP97 (Figures 5B3 and 5C3) suggest that these SAP97 constructs potentiate EPSC by delivering new GluR1-containing AMPARs to the synapse. In this context, it is striking that the I38G mutant decreased the synaptic response amplitude (Figure 5A3) at the same time that it increased rectification (Figure 5A4). Thus a multimerization-competent L27 domain is not needed to drive GluR1 into synapses but is required to strengthen synaptic transmission.

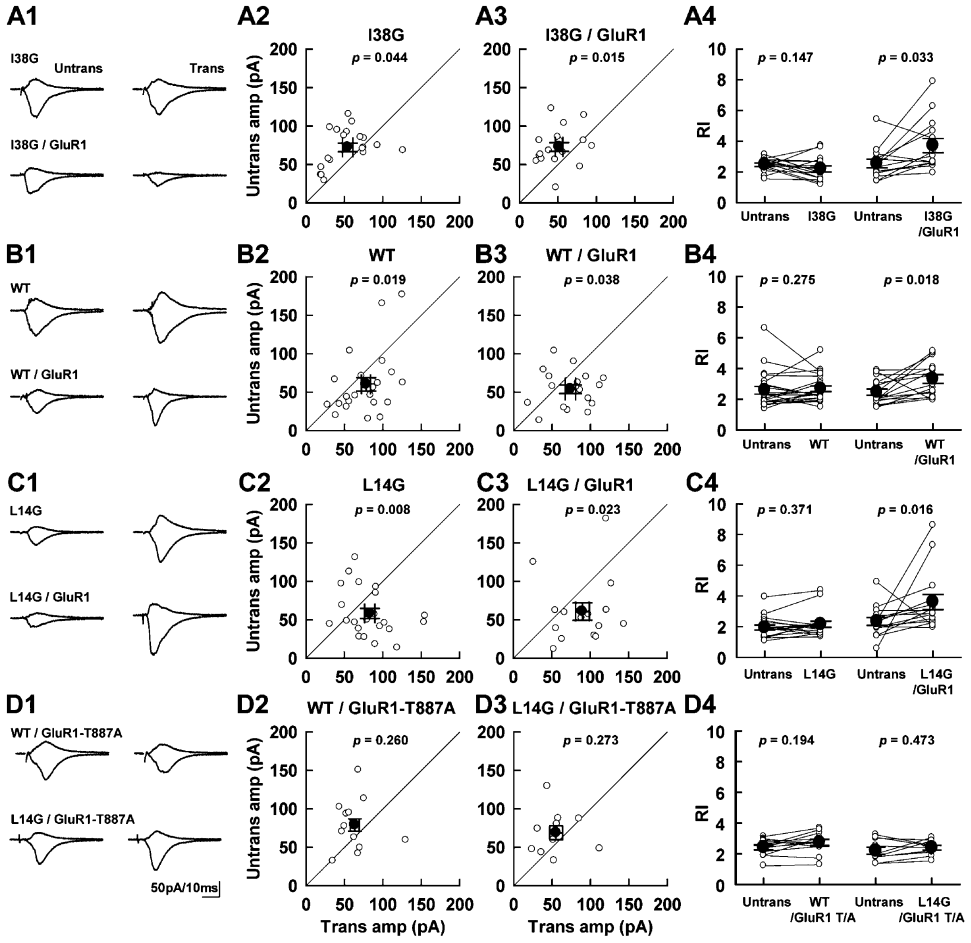


Figure 5. SAP97 Overexpression Delivers GluR1 AMPAR to the Synapse

Neurons were transfected with wild-type or I38G- or L14G-SAP97 with or without GluR1, and AMPAR EPSCs were recorded in the presence of NMDAR blocker at both −60 mV and +40 mV to obtain the rectification index. (A1–D1) Sample traces. (A2–C2 and A3–C3) Plot of AMPAR EPSC amplitude from neurons expressing SAP97 constructs with GluR1 (A3–C3) or without GluR1 (A2–C2) at −60 mV. (A4–C4) Comparison of rectification index between untransfected and transfected neurons. Open circles connected with lines represent individual pairs of cells, and filled circles represent averages ± SEM. (Left) Neuronal pairs transfected only with SAP97. (Right) Cotransfection of SAP97 and GluR1. Overexpression of SAP97-I38G reduced synaptic transmission but still increased RI (A), indicating delivery of GluR1 to synapse. Overexpression of wild-type SAP97 (B) or L14G-SAP97 (C) enhanced synaptic transmission and increased RI, indicating delivery of GluR1. Wild-type or L14G-SAP97 did not increase synaptic response or RI when coexpressed with C-terminal mutant GluR1-T887A (D). Numbers of AMPAR EPSCs and RI recordings were I38G (AMPAR/RI: 19/15), I38G/GluR1 (17/14), SAP97 (23/22), SAP97/GluR1 (18/18), L14G (22/17), L14G/GluR1 (15/15), SAP97/GluR1-T887A (12/12), and L14G/GluR1-T887A (10/10).

The GluR1 C-terminal mutant (GluR1-T887A) cannot bind SAP97 (Cai et al., 2002). When coexpressed with GluR1-T887A, neither wild-type SAP97 nor L14G was able to increase AMPAR EPSCs or rectification (Figure 5D). These findings indicate that the PDZ binding motif of GluR1 is required for SAP97-mediated GluR1 incorporation into the synapse, perhaps through binding to SAP97. The GluR1-T887A mutant appears to have a "dominant interfering" action on endogenous AMPA receptors, because SAP97 no longer potentiated AMPAR EPSCs in cells cotransfected with this GluR1 mutant (Figures 5D2 and 5D3).

### SAP97 Multimerization and Spine Turnover

Given its potential role in GluR1 trafficking to the synapse, we studied the dynamics of SAP97 in neurons. One day after transfection into hippocampal neurons, YFP-tagged SAP97 (wild-type, I38G, or L14G) was enriched in spines, albeit less markedly than PSD-95 (Figure 6A). According to time-lapse confocal imaging, individual SAP97-YFP puncta associated with spines did not change in position or fluorescence intensity over a time course of 10 min (Figure 6B). To measure dynamics of SAP97 turnover in spines, we photobleached YFP-SAP97 within single spines and followed the fluorescence recovery after photobleaching (FRAP) (Figures 6C and 6D). The fluorescence recovery rate of I38G (time constant $\tau = 1.42$ min) was faster than that of wild-type ($\tau = 1.60$ min) or L14G ($\tau = 1.82$ min). None of these SAP97 variants recovered to the prebleached level of fluorescence, suggesting the presence of an immobile intraspinal population of these molecules that does not exchange within a few minutes. Wild-type SAP97 (58%) and L14G mutant (59%) recovered to a lesser extent than

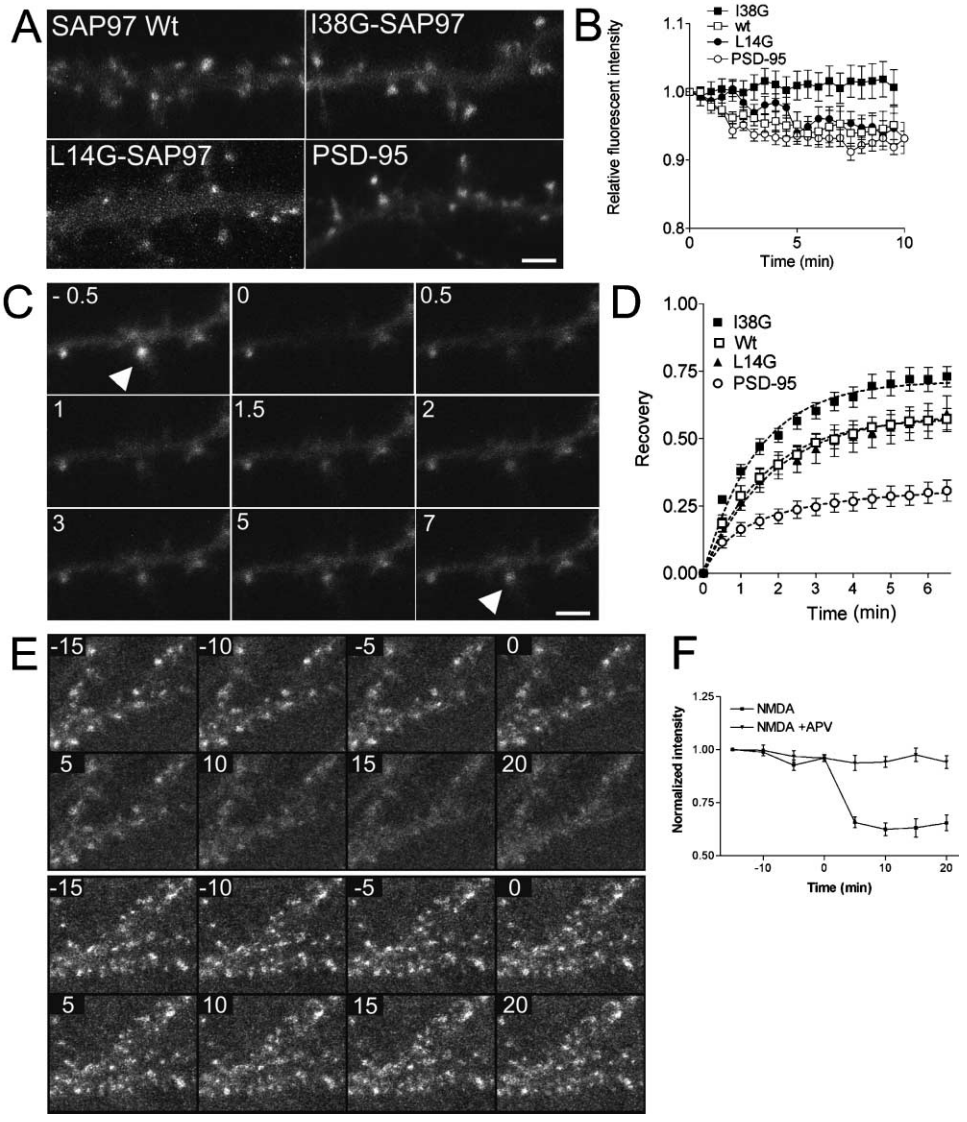


Figure 6. Dynamics of SAP97 Variants and PSD-95 in Dendritic Spines

(A) Distribution of YFP-tagged SAP97, I38G-SAP97, L14G-SAP97, and PSD-95 in dendrites of cultured hippocampal neurons. All constructs show spine enrichment accompanied by weak diffuse signal in the dendritic shaft (scale bar, 1.6 μm).

(B) Change in fluorescence intensity in individual spines (mean ± SEM) during time-lapse imaging (images captured every 0.5 min). Values were normalized to t = 0. Number of spines recorded: 63 (SAP97), 80 (I38G-SAP97), 57 (L14G-SAP97), and 86 (PSD-95).

(C) Fluorescence recovery after photobleaching (FRAP) in a spine of a neuron overexpressing YFP-tagged wild-type SAP97. Images were taken every 0.5 min for 7 min. Arrowhead indicates bleached spine. Numbers in each panel indicate number of minutes following bleaching (scale bar, 1.75 μm).

(D) Time course of FRAP for wild-type and mutant SAP97 and PSD-95 (mean ± SEM) in dendritic spines. Dotted lines are regression curves that are fit to single exponential associations (SAP97 Wt, I38G, and L14G) or hyperbola (PSD-95). Number of spines recorded: 10 (SAP97), 11 (I38G-SAP97), 9 (L14GS-AP97), and 16 (PSD-95).

(E) DIV 18–21 neurons infected with lentivirus expressing YFP-SAP97 were stimulated with 3 μM NMDA (upper panel) or 3 μM NMDA + 100 μM APV (lower panel). Numbers indicate time in minutes relative to NMDA stimulation.

(F) Time course of change in fluorescence intensity of YFP-SAP97 in dendritic spines following NMDA stimulation (normalized to t = 15 min before NMDA stimulation) (number of neurons imaged: 7 [NMDA], 5 [NMDA + APV]).

did I38G-SAP97 (71%), implying that a larger fraction of wild-type and L14G-SAP97 lies "immobile" in the spine. Thus a multimerization-competent L27 domain is associated with increased stability of SAP97 in spines. Under the same experimental conditions, PSD-95-YFP showed a lower FRAP rate than did SAP97 and a much lower recovery level at 6 min after photobleaching (35%; Figure 6D). These results are consistent with the idea that PSD-95, but not SAP97, is a stable scaffold of the PSD.

Since AMPAR trafficking is regulated by activity, we examined the influence of NMDAR activation on SAP97 distribution. Lentiviral vectors (Lois et al., 2002) were

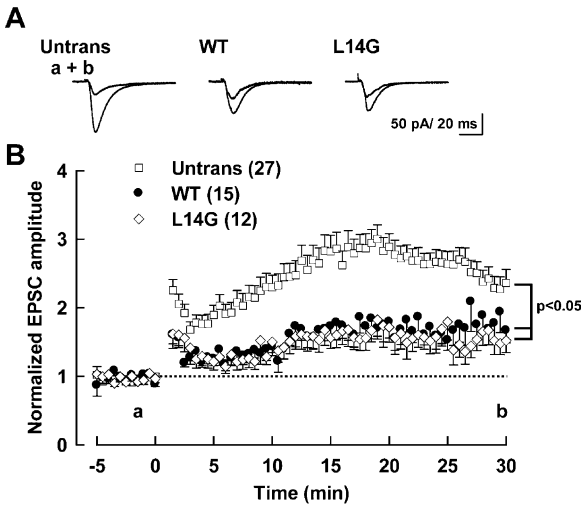


Figure 7. Overexpression of SAP97 Partially Occludes LTP

LTP was induced in CA1 neurons of hippocampal slice cultures by pairing depolarization to 0 mV with 2 Hz stimulation for 100 s. (A) Sample AMPAR EPSC traces from untransfected neurons and neurons transfected with wild-type or L14G-SAP97. Currents before and after pairing are superimposed. (B) Time course of AMPAR EPSCs after LTP induction (pairing protocol was delivered at t = 0). The time points at which sample traces were obtained are indicated by a and b. Numbers in parentheses indicate number of cells.

used to achieve high-efficiency transfection and optimal levels of expression of YFP-SAP97 in dissociated cultured neurons, with minimal cytotoxicity. Treatment with 3 μM NMDA dispersed YFP-SAP97 from spines within 5–10 min, and APV (100 μM) blocked this effect (Figures 6E and 6F). Because bath application of NMDA typically causes LTD and loss of surface AMPAR in cultured neurons, the rapid dispersal of SAP97 from postsynaptic sites is consistent with a role for SAP97 in activity-dependent AMPAR trafficking.

### LTP Occlusion by SAP97

Does SAP97-induced enhancement of AMPAR EPSC share any mechanism with LTP? After induction, untransfected neurons displayed stable LTP (>2-fold enhancement of EPSC) lasting for ≥30 min (Figure 7). Cells expressing wild-type or L14G-SAP97, which by themselves potentiate AMPA currents (Figures 4 and 5), showed much smaller LTP responses than did untransfected cells (Figure 7). The effect of I38G-SAP97 on LTP was not tested because this mutant has significant negative effects on NMDAR EPSC (see Figure 4A). Since L14G-SAP97 mutant clearly does not affect NMDAR EPSC (see Figure 4C), the inhibition of LTP by SAP97 is unlikely to be due to inhibition of the NMDAR current. Rather, the occlusion of LTP by SAP97 probably results from the synaptic delivery of GluR1-containing AMPARs, a mechanism that is common to SAP97-induced potentiation and LTP.

### Effect of SAP97 RNAi on Synaptic Transmission and Surface AMPAR

The functional analysis of SAP97 has so far relied on approaches involving overexpression. Therefore we turned to RNAi to evaluate the physiological role of endogenous SAP97 in hippocampal slice cultures. RNAi knockdown of PSD-95 was performed in parallel to compare the effects and to verify the specificity of the loss of function. Small interfering RNA (siRNA) was introduced into cells by transfection using a plasmid (pSuper)-based system (Brummelkamp et al., 2002). A 19 nucleotide sequence from rat SAP97 (pSuper4-34) and PSD-95 (pSuper2-16) suppressed the expression of endogenous SAP97 and PSD-95, respectively, in hippocampal neurons (Supplemental Figure S3 [http://www.neuron.org/cgi/content/full/44/3/453/DC1/]). When transfected in CA1 neurons of hippocampal slice cultures, SAP97 RNAi caused a significant decrease in both AMPAR and NMDAR EPSCs (Figures 8B and 8D), while empty vector (pSuper) had no effect (Figures 8A and 8D). In contrast, RNAi of PSD-95 reduced only the AMPAR current, with no effect on NMDARs (Figures 8C and 8D).

Dissociated neurons transfected with SAP97 RNAi plasmid for 3 days showed a significant reduction in the density of dendritic protrusions (protrusion density per 10 μm of dendrite was 6.53 ± 0.31 [pSuper control] and 5.48 ± 0.33 [SAP97 RNAi]; $p < 0.001$). In addition, we observed a decreased density of excitatory synapses, as measured by PSD-95 puncta density (PSD-95 puncta per 10 μm was 8.38 ± 0.65 [pSuper control] and 5.98 ± 0.25 [SAP97 RNAi]; $p < 0.001$) (data not shown). Therefore, reduction of both AMPAR- and NMDAR EPSCs by SAP97 RNAi may correlate with a depletion of synapses. Protrusion density per 10 μm of dendrite was also decreased in neurons overexpressing I38G-SAP97 (5.31 ± 0.35; $p < 0.001$) but not wild-type SAP97 (6.42 ± 0.31) or GFP control (6.31 ± 0.38; data not shown).

To quantify the effects of SAP97 RNAi at a biochemical level across the entire population of neurons in culture, we constructed lentiviral vectors for expressing specific siRNAs (Figure 9A; see Experimental Procedures). Nearly 100% of neurons in culture can be infected with lentivirus with minimal cytotoxicity. Compared to empty virus infection at the same viral titer, lentivirus expressing SAP97 siRNA or PSD-95 siRNA caused profound and specific knockdown of SAP97 and PSD-95, respectively, as shown by immunoblotting of total lysates of hippocampal cultures (Figure 9B). Surface biotinylation assays were performed to measure the surface versus the total protein levels of GluR1 and GluR2 (Ehlers, 2000; Lin et al., 2000). Knockdown of either SAP97 or PSD-95 reduced total GluR1 and total GluR2 to similar extents (~20%–30% reduction compared with empty vector; Figures 9B and 9C). Surface GluR1 was decreased by ~25% by PSD-95 RNAi (similar to the decrease in total GluR1) and by 50%–60% by SAP97 RNAi (Figures 9B and 9C). The surface GluR2 level was strongly reduced (~50%) by SAP97 RNAi but was relatively unaffected by PSD-95 knockdown. Thus SAP97 is required to support the surface expression of both GluR1 and GluR2, whereas PSD-95 is needed specifically for surface GluR1. In addition to affirming the specificity of RNAi effects in this system, these loss-of-function data reveal the overlapping but distinct roles of SAP97 and PSD-95 in synapses.

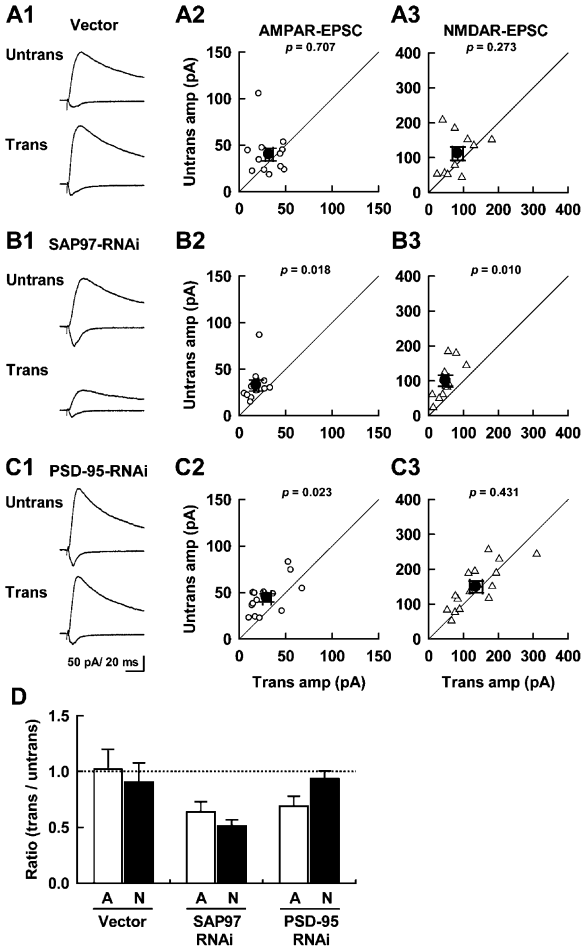


Figure 8. Differential Effects of RNAi of SAP97 and PSD-95 on Synaptic Transmission

Synaptic responses were measured in cultured hippocampal slices transfected with control (vector), SAP97, or PSD-95 RNAi constructs. (A1–C1) Sample EPSC traces mediated by AMPAR (downward trace) and NMDAR (upward trace) from pairs of transfected (Trans) and neighboring untransfected (Untrans) cells. Scale bar, 50 pA, 20 ms. (A2–C2 and A3–C3) EPSC amplitudes (AMPAR EPSC and NMDAR EPSC) were plotted for each pair of transfected (Trans) and neighboring untransfected (Untrans) cells. Individual open symbol represents a single pair of recordings; filled circles show mean ± SEM. (D) Quantitation of effects of vector control, SAP97 RNAi, or PSD-95 RNAi on AMPA (white bars) and NMDA EPSCs (black bars) is shown as a ratio between transfected/untransfected neurons. Transfection of pSuper vector (A) did not change the amplitude of either AMPAR or NMDAR EPSCs. SAP97 RNAi reduced both AMPAR and NMDAR EPSCs (B), whereas PSD-95 RNAi specifically inhibited AMPAR EPSC with no effect on the NMDAR component (C). Numbers of EPSC recordings were as follows: vector (AMPAR/NMDAR: 12/10); SAP97 RNAi (11/11); and PSD-95 RNAi (15/14).

## Discussion

### EM Structure of MAGUK Scaffolds

Knowing the molecular structure of PSD-95 and SAP97 would be useful to understanding the structure-function relationships of these important scaffolds. EM images of SAP97 have been obtained by low-angle rotary shadowing but have provided limited structural information (Marfatia et al., 2000). Using negative-stain EM combined with computer-aided averaging, we obtained higher-resolution structures that revealed the surprisingly different shapes of monomeric full-length PSD-95 and SAP97. PSD-95 had a compact C-shaped conformation, whereas SAP97 preferentially adopted an extended rod-like conformation. A minority of SAP97 monomers showed an alternative C-shape configuration similar to that seen for PSD-95, consistent with previous structural modeling of SAP97 (Wu et al., 2000).

Our EM data on PSD-95 and SAP97 indicate that MAGUK scaffolds have preferred conformations as full-length proteins, debunking the concept of multidomain scaffold proteins as flexible "beads on a string." The proper geometric organization of domains within MAGUK proteins may be important for their scaffold function, since scrambling the order of individual protein interaction modules in STE5, a yeast scaffold protein for a MAP kinase pathway, has been shown to disrupt signaling efficacy (Park et al., 2003).

In addition to differences in shape between their monomers, SAP97 and PSD-95 exhibited distinct quaternary structures. Soluble SAP97 tended to dimerize, whereas PSD-95 was primarily monomeric. Differences in structure and multimerization could underlie the functional distinctions between PSD-95 and SAP97, for example, by determining the selectivity of binding partners. Scaffold multimerization is proposed for another multi-PDZ protein, GRIP, although the functional significance is unclear (Srivastava et al., 1998). Multiple splice variants exist for SAP97 and PSD-95, and it remains to be determined how differential splicing affects the structure-function of these MAGUK scaffolds.

$K^+$ channels are binding partners of PSD-95 and SAP97 (Kim et al., 1995; Tiffany et al., 2000), and a tetrameric $K^+$ channel has dimensions of approximately 100 Å × 100 Å (Jiang et al., 2003; Sokolova et al., 2001). The size of a tetrameric AMPAR is estimated as 110 Å × 140 Å by negative-stain EM (Safferling et al., 2001). A compactly folded C-shaped PSD-95 (~100 Å × 60 Å) is comparable in size to these tetrameric receptor/channels and could fit comfortably below the $K^+$ channel or a glutamate receptor. In contrast, SAP97 in its preferred rod-like conformation (150 Å in length) can potentially extend beyond its bound receptor or channel, if it lies parallel to the membrane.

### L27 Domain and SAP97 Dynamics

We show here that the L27 domain mediates multimerization of SAP97, in keeping with a study of the human homolog hDlg (Marfatia et al., 2000). Although our study focused on homomultimerization, it is likely that SAP97 also heteromultimerizes with other L27-containing proteins such as CASK, DLG2, and DLG3 (Karnak et al., 2002). The motor protein myosin-6 also interacts with the L27 domain of SAP97 (Wu et al., 2002). The critical amino acids for self-association that we identify in the SAP97 L27 domain overlap the residues that are important for heteromultimerization between Pals1 (mLin-7) and PATJ (Roh et al., 2002). Therefore, our experiments in neurons do not distinguish between effects of L27 mutations on heteromultimerization versus homomultimerization of SAP97. Nevertheless, the conclusion holds that a multimerization-competent L27 domain is

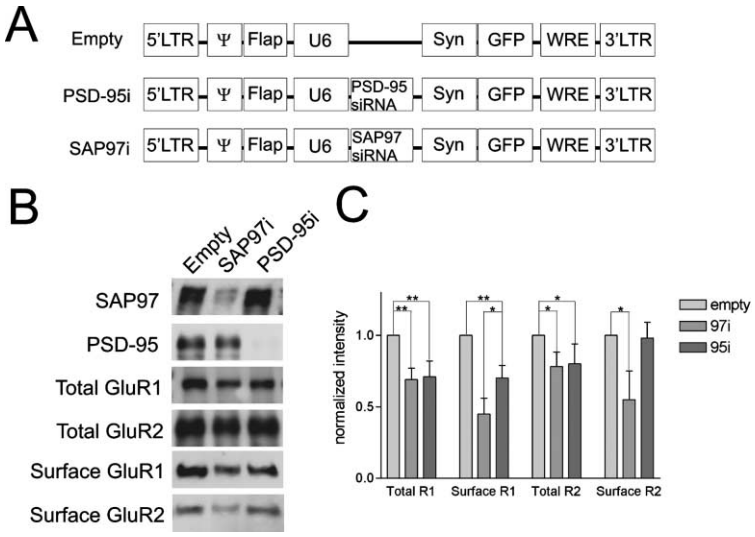


Figure 9. RNAi Knockdown of SAP97 Decreases Surface AMPA Receptors

(A) Diagram of lentivirus vector for RNAi. LTR, long terminal repeat; Ψ, packaging signal; Flap, flap element from HIV-1; U6, U6 promoter; Syn, synapsin promoter; WRE, woodchuck hepatitis virus posttranscriptional regulatory element.

(B) Representative immunoblot for SAP97, PSD-95, and total and surface GluR1 and GluR2 in hippocampal neurons infected with control (empty) lentivirus or lentivirus expressing siRNA against SAP97 (SAP97i) or PSD-95 (PSD-95i). Surface GluR1/GluR2 were isolated by surface biotinylation and subsequent streptavidin purification.

(C) Quantification of protein changes induced by SAP97 or PSD-95 RNAi (based on densitometric measurements of immunoblots such as shown in (B). *$p < 0.05$, **$p < 0.01$, $n = 5$.

important for stability of SAP97 in spines and for synaptic potentiation by SAP97. In this context, it is noteworthy that CaMKII can phosphorylate serine-39 in the L27 domain of SAP97 and promotes SAP97 targeting to dendritic spines (Mauceri et al., 2004).

In dendritic spines, the turnover rate of SAP97 is faster than that of PSD-95, consistent with an association of SAP97 with highly mobile AMPARs. L27 domain mutations that disrupt multimerization resulted in faster turnover of SAP97 in spines. Interestingly, these mutations disabled SAP97 with respect to synaptic potentiation but not with respect to GluR1 delivery. One possible explanation is that disruptive L27 mutations shift the equilibrium of SAP97, favoring the "dynamic monomer" capable of trafficking GluR1 to the synapse but reducing the "immobile multimer" responsible for stabilizing AMPARs at the synapse.

If SAP97 is involved in AMPAR trafficking, it might be expected to show activity-regulated movement in neurons. Indeed, we observed NMDA-induced redistribution of YFP-SAP97 in cultured neurons, but away from, rather than toward, spines. This finding is consistent with the fact that bath application of NMDA typically elicits loss of surface AMPARs and LTD in cultured neurons (Beattie et al., 2000; Carroll et al., 2001; Ehlers, 2000). A similar activity-dependent dispersal of PSD-95 from synapses has also been reported, involving depalmitoylation of N-terminal cysteines in PSD-95 (El-Husseini et al., 2002). However a time-lapse study indicated little evidence of activity-dependent dynamics of PSD-95-GFP between the spine and the shaft (Okabe et al., 2001). Further studies are needed to examine whether LTP-inducing stimuli can provoke the translocation of SAP97 to synapses.

SAP97 is concentrated in the ER and has been proposed to convey AMPAR from ER to the cell surface (Sans et al., 2001). According to this model, at least part of SAP97 should associate with intracellular membrane compartments that contain AMPARs. We were unable to detect YFP-SAP97 moving as puncta within dendrites or into/out of spines, but this could be due to insufficient resolution or the signal-to-noise limitations of our time-lapse imaging.

### Role of SAP97 in Synaptic Function

We show here that overexpression of SAP97 (unburdened by GFP or epitope tags) robustly enhanced synaptic AMPA currents, with little effect on the NMDA component. These results are consistent with a role for SAP97 in synaptic trafficking of GluR1 receptors (Hayashi et al., 2000; Rumbaugh et al., 2003; Sans et al., 2001). Our findings differ from those of a previous report in which no effect was found with overexpression of SAP97 that was tagged at its C terminus with GFP (Schnell et al., 2002). Given that SAP97 and PSD-95 fold in specific conformations, their structure/function could be sensitive to the insertion of large moieties like GFP. Based on the crystal structure and mutational analysis, the extreme C terminus of PSD-95 family proteins plays a role in the intramolecular interactions between SH3 and GK domains (McGee and Bredt, 1999; McGee et al., 2001; Shin et al., 2000; Tavares et al., 2001). Because the C terminus of SAP97 is buried within the hydrophobic pocket between the SH3 and GK domains (McGee et al., 2001; Tavares et al., 2001), attaching GFP to this segment could hinder the folding of the SH3/GK domain and impair the function of SAP97. An N-terminal GFP tag, however, appeared not to affect synaptic targeting of SAP97 (Rumbaugh et al., 2003).

In a recent study, overexpression of N-terminally-tagged GFP-SAP97 in dissociated neurons increased the frequency but not the amplitude of mini-EPSCs (Rumbaugh et al., 2003). While this result can be explained by a postsynaptic mechanism (such as increased number of postsynaptically functional synapses), it seems at odds with the increase in average size of GluR1 clusters induced by SAP97 (Rumbaugh et al., 2003). Our electrophysiological data establish that SAP97 potentiates evoked synaptic responses in a more intact preparation (slice culture) and provide strong evidence that SAP97 acts at the postsynaptic locus to strengthen synapses (delivery of GluR1, no change in PPF, and increase in mEPSC amplitude).

How does SAP97 increase synaptic strength? A prevailing model of synaptic plasticity is based on GluR1-containing AMPARs being recruited to synapses during NMDAR-dependent LTP (Hayashi et al., 2000; Passafaro

et al., 2001; Shi et al., 1999). Our electrophysiological data show that SAP97 can "drive" homomeric GluR1 into synapses and partially occlude LTP, implying that SAP97 acts upon a GluR1 pathway in common with LTP to effect synaptic strengthening. In this regard, SAP97 behaves like PSD-95, albeit less potently (Ehrlich and Malinow, 2004; Schnell et al., 2002; Stein et al., 2003). It is therefore of particular significance that I38G-SAP97 causes synaptic accumulation of GluR1 (as evidenced by increased rectification) but without synaptic potentiation (indeed, I38G slightly inhibits AMPAR EPSCs). The molecular dissociation of these two effects implies that synaptic potentiation involves more than synaptic delivery of GluR1 AMPARs. As discussed above, the monomeric form of SAP97 appears sufficient to deliver GluR1 to synapses, while L27-mediated interactions of SAP97 may be required to stabilize synaptic AMPARs once they are delivered. This "two-step" function is reminiscent of the stargazin family of proteins, which associate with AMPARs and are critical for synaptic expression of AMPARs by binding to PSD-95 (Chen et al., 2000; Tomita et al., 2003). It will be interesting to investigate the involvement of stargazin in SAP97-mediated trafficking of GluR1.

RNAi knockdown of SAP97 inhibits the AMPAR EPSC as effectively as does PSD-95 RNAi, supporting the idea that SAP97 is normally involved in delivery and/or stabilization of synaptic AMPARs. The unexpected finding was that RNAi of SAP97 also decreased NMDAR currents, whereas knockdown of PSD-95 inhibited only the AMPAR component. The latter result supports the idea that PSD-95 is not essential for synaptic targeting of NMDAR (Migaud et al., 1998; Passafaro et al., 1999; Sprengel et al., 1998). A broader role for SAP97 in synaptic function is also evidenced by the inhibitory effect of overexpressed SAP97-I38G on NMDAR currents and on dendritic protrusion density, which we interpret as dominant-interfering effects reflecting again the importance of the L27 domain in SAP97 activity.

How does loss of SAP97 lead to reduced NMDAR currents? One obvious possibility is that SAP97 is also involved in the synaptic delivery or stabilization of NMDARs, since, at least in vitro, the C termini of NMDAR NR2 subunits can bind to the PDZ domains of SAP97 (Niethammer et al., 1996; Songyang et al., 1997). Association of SAP97 with NMDARs in brain has been reported by some (Gardoni et al., 2003) but not others (Sans et al., 2001). An alternative explanation is that SAP97 is more generally important for synapse growth and/or maintenance. It is likely that SAP97 binds to numerous proteins in addition to GluR1. Along with AMPARs, SAP97 may be required for trafficking other (structural or signaling) proteins needed for synaptic growth/maintenance. Consistent with this idea, RNAi of SAP97 reduced the density of dendritic protrusions. Thus, loss of NMDARs following depletion of SAP97 could be an indirect consequence of loss or shrinkage of synapses. It should be stressed, however, that the potentiating effect of SAP97 overexpression is unlikely due to the formation of more synapses, because AMPAR EPSCs were selectively enhanced, resulting in increased AMPA/NMDA ratios. Thus SAP97 has a relatively specific function in AMPAR trafficking.

In conclusion, our results show that SAP97 enhances synaptic strength, dependent on L27 domain-mediated interactions. SAP97 functions, at least in part, by promoting the synaptic delivery of GluR1-containing AMPA receptors. However, our data also imply additional roles for SAP97 in maintaining the functional and morphological integrity of synapses. The identification of the other components of the SAP97 protein complex will be helpful for understanding the mechanisms of synaptic growth and plasticity.

## Experimental Procedures

### Recombinant DNA

L27 domain was defined as amino acids 1–65 (MPVRK…LDNPK) of SAP97. The ΔL27 construct starts from amino acid 66 (CVDHS…); hexahistidine tag (6xHis) was inserted at the N terminus, supplying the first methionine.

#### *Baculoviral Constructs*

PSD-95 and PSD-95-EGFP tagged with C-terminal 6xHis were cloned into pBacdPAK8 (Clontech). SAP97 with N-terminal 6xHis was cloned into pBacPAK9. SAP97 point mutants were generated by in vitro mutagenesis with the QuickChange kit (Stratagene) and cloned into pFastBac1 (GIBCO).

#### *Mammalian Expression Constructs*

PSD-95-YFP/CFP and YFP/CFP-SAP97 were cloned into β-actin promoter vector. Untagged I38G- and L14G-SAP97 were cloned into expression vector pGW1, as were SAP97 and PSD-95 (Kim et al., 1995).

### Baculovirus Protein Production

Recombinant baculoviruses were produced using BacPAK6 (Clontech) or Bac-to-Bac system (GIBCO). Sf9 cells were infected with the virus at MOI = 5 and harvested 48 hr postinfection. Cells were lysed in buffer A (20 mM Tris HCl pH 9.0, 500 mM NaCl, 20 mM imidazole, 20 mM β-mercaptoethanol, plus protease inhibitors) by Dounce homogenization and centrifuged at 50,000 rpm at 2°C for 15 min. Supernatant was loaded on a $Ni^{2+}$ chelating Sepharose column and eluted with buffer A containing 250 mM imidazole. The peak fraction was desalted with a PD-10 column (Pharmacia), applied to Mono Q HR 5/5 (Pharmacia), and eluted with linear salt gradient produced between buffer L (20 mM Tris HCl pH 9.0, 100 mM NaCl, 5 mM DTT) and buffer H (20 mM Tris HCl pH 9.0, 1 M NaCl, 5 mM DTT). Peak fraction was concentrated by Ultrafree (Millipore) and further purified by Superdex200 (Pharmacia) in buffer C (20 mM Tris HCl pH 8.0, 150 mM NaCl, 5 mM DTT).

### Analytical Gel Filtration

Superdex200 5/5 HR column (Pharmacia) was pumped by AKTA FPLC (Pharmacia) at a flow rate of 0.5 ml/min. Protein samples (100 μl) (0.5–1 mg/ml) were loaded and the elution profile was monitored by absorbance at 280 nm. The column was precalibrated using MW standards (Pharmacia) of known Stokes' radius (see Figure 3). Stokes' radius was determined by plotting Kav versus log (MW), where Kav = (Ve − Vo)/(Vt − Vo); Vo = void volume; Ve = elution volume; Vt = total column bed volume. The native molecular weight was derived from equation $M = \alpha aS$, where a = Stokes' radius, S = sedimentation coefficient. $\alpha = 6\pi\eta N/(1 - \upsilon\rho)$, where $\eta$ = viscosity of the solvent, N = Avogadro's number, $\upsilon$ = partial specific volume of the protein, and $\rho$ = density of solvent (Siegel and Monty, 1966).

### Electron Microscopy and Image Processing

PSD-95 or SAP97 solution (5 μl) (0.05–0.1 mg/ml) was applied to a glow-discharged carbon-coated grid and negatively stained with uranyl formate as described (Ohi et al., 2004). Samples were inspected with a FEI Philips T12 transmission EM and images were taken at a nominal defocus of −1.5 μm using low-dose procedures. Images were digitized with a Zeiss SCAI scanner using a step size of 7 μm, and 3 × 3 pixels were averaged yielding a pixel size of 4 Å on the specimen level. The SPIDER suite of programs was used for image processing (Frank et al., 1996). Particles were windowed into 80 × 80 pixel images. The images were subjected to several rounds

of alignment, multivariate statistical analysis, classification, and image averaging.

### Analytical Ultracentrifugation

An Optima XL-A centrifuge (Beckman) was operated with an An-Ti60 rotor. A double-sector cell, equipped with a 12 mm Epon centerpiece and quartz windows, was loaded with ~400 μl of protein sample (0.3–0.6 mg/ml). Data were collected at rotor speeds of 3000–60,000 rpm in continuous mode at 10°C, with a step size of 0.005 cm and an average of three scans per point. The sedimentation velocity absorbance profiles were analyzed using the DCDT software provided by J.S. Philo (Philo, 1997) to obtain the apparent distribution of sedimentation coefficients $g(s^*)$. The partial specific volume value of 0.71 $cm^3/g$ was determined based on the PSD-95 and SAP97 amino acid sequence.

### Chemical Crosslinking of Purified Proteins

Purified proteins were dialyzed against phosphate-buffered saline (PBS) and ultracentrifuged. Gel filtration elution profiles were indistinguishable after buffer exchange. The crosslinking reaction was carried out at room temperature by mixing 30 μl (0.2 mg/ml) of protein and 30 μl of glutaraldehyde (0.04%–0.0012% in PBS, freshly prepared) and terminated after 20 min by 10 μl of 1M Tris-HCl, pH 7.4.

### Antibodies and Immunocytochemistry

The following primary antibodies were used: mouse monoclonal PSD-95 antibody K28/43 (a gift from J. Trimmer; State University of New York, Stony Brook, NY); polyclonal GluR2/3 C-terminal antibody AB1506, polyclonal GluR1 C-terminal antibody AB1504 (Chemicon, Temecula, CA); polyclonal GluR1 N-terminal antibody Ab-1 (Oncogene Research Products); monoclonal β-gal antibody (Promega); polyclonal β-gal antibody Ab616-1000 (Abcam). Polyclonal SAP97 N-terminal antibody has been described previously (Kim et al., 1996). Polyclonal antibody against SAP97 was raised against purified SAP97 expressed in Sf9 cells. The antibody was affinity-purified with a SAP97-conjugated CNBr-Sepharose column (Pharmacia) and further preabsorbed with PSD-95-conjugated CNBr Sepharose. Immunocytochemistry of hippocampal cultures was performed as described (Sala et al., 2003).

### Lentiviral Vectors and Surface Biotinylation Experiment

Lentiviral vectors were produced according to Lois et al. (2002). YFP-SAP97 was subcloned into plasmid FSW, which is the same as FUGW (Lois et al., 2002) except that the ubiquitin promoter and GFP were replaced with the synapsin promoter. For lentiviral RNAi, the ubiquitin promoter of pLL3.7 (Rubinson et al., 2003) was replaced with the synapsin promoter. The following siRNA sequences were used: SAP97, 5′-GATATCCAGGAGCATAAAT-3′; PSD-95, 5′-GCCTT CGACAGAGCCACGA-3′. Neurons were infected with RNAi-lentivirus (5 μl of $10^8$ cfu/ml) at DIV10-12 and surface biotinylated 5–7 days later, as described by Lin et al. (2000).

### Live Imaging

FRAP: An LSM510 confocal system mounted on Axiovert 2M (Zeiss) was used. Transfected or infected neurons (DIV15) cultured on coverglass were mounted on a 37°C metal holder prior to imaging. Neurons were preincubated in Tyrode's solution (145 mM NaCl, 3 mM KCl, 10 mM HEPES, 10 mM glucose, 5 μM glycine, 2.6 mM $CaCl_2$, 1.3 mM $MgCl_2$, pH 7.4, 310 mosm) for 15 min before imaging and maintained in the same solution at 37°C during imaging (100× NA1.3 objective). Automatic image acquisition was obtained with Time series software (Zeiss), with excitation and photobleaching at 488 nm and 513 nm, respectively. Spines clearly isolated from the shaft of the dendrite were manually selected for photobleaching. Background and photobleaching effects caused by continuous imaging were corrected for in quantification.

FRET: FRET was detected as described (Okamoto et al., 2004). YFP was photobleached with light from a mercury lamp (100 W) through a filter set specific for YFP excitation (excitation filter: 525/45; dichroic mirror: 570 long-pass). Neurons were maintained in Tyrode's solution at 25°C during imaging.

### Electrophysiology

Electrophysiological recordings were carried out from organotypic slice cultures as described (Sala et al., 2003). Neurons were transfected using a biolistic gene gun (Bio Rad) at DIV 3–6 (100 μg DNA; 90% of the construct to test; 10% pEGFP-C1). pCI-GluR1, pGW1-SAP97, and pEGFP-C1 constructs were transfected at the ratio of 45:45:10. Electrophysiological recordings were performed at 2–3 days (overexpression) and 3–4 days (RNAi) after transfection. Recordings were carried out in solution containing NaCl, 119 mM; KCl, 2.5 mM; $CaCl_2$, 4 mM; $MgCl_2$, 4 mM; $NaHCO_3$, 26 mM; $NaH_2PO_4$, 1 mM; glucose, 11 mM; picrotoxin, 0.15 mM; and 2-chloroadenosine, 0.003 mM for LTP experiments and 0.01 mM for others, gassed with 5% $CO_2$/95% $O_2$, at pH7.4. Whole-cell recordings were made simultaneously from a pair of CA1 pyramidal neurons, one transfected and one untransfected, during stimulation of presynaptic fibers at 0.2 Hz. In most recordings, except LTP and asynchronous synaptic events, we stimulated two independent synaptic inputs. In such cases, we averaged the amplitudes of these two inputs and counted them as "n = 1." Synaptic AMPA receptor responses were recorded at −60 mV and NMDA receptor responses were recorded at +40 mV in the presence of NBQX (0.01 mM). The rectification index (RI) was calculated as the ratio of the AMPAR EPSCs amplitude at −60 and +40 mV in the presence of 100 μM DL-APV, 1 μM CPP, and 10 μM bicuculline. LTP was induced by pairing 2 Hz stimulation with depolarization of the postsynaptic cell to 0 mV for 100 s. For recording of the $Sr^{2+}$-induced asynchronous synaptic current, $CaCl_2$ was replaced with 4 mM $SrCl_2$, and 2-chloroadenosine was removed. Events larger than 5 pA were included. Experiments were blinded in regard to the DNA constructs used. Results are reported as mean ± SEM. Statistical significance was evaluated with Kruskal-Wallis ANOVA (Figures 4E and 7), the Kormogorov-Smirnov test (Supplemental Figure S2 [http://www.neuron.org/cgi/content/full/44/3/453/DC1/]), and the Mann-Whitney test (others).

### RNAi

The following siRNA sequences were subcloned into pSuper (Brummelkamp et al., 2002): SAP97, 5′-CCCAAATCCATGGAAAATA-3′; PSD-95, 5′-GCCTTCGACAGAGCCACGA-3′. RNAi plasmids were transfected by calcium phosphate method (for dissociated neurons) or by gene gun (slice cultures).

### Acknowledgments

The molecular EM facility at Harvard Medical School was established by a donation from the Giovanni Armenise Harvard Center for Structural Biology and is maintained by NIH grant GM62580. We thank Atsushi Miyawaki for Venus cDNA; Tsutomu Hashikawa for support; Carlos Lois for reagents and advice for lentiviral experiments; Michael T. McManus for pLL3.7; and Benny Chih and Peter Scheiffele for synapsin promotor. K.F. is a recipient of a Special Postdoctoral Researchers Fellowship from RIKEN. Y.H. is in part supported by Ellison Medical Foundation. T.N. was supported by Human Frontier Science Program Long Term Fellowship. M.S. is an investigator at Howard Hughes Medical Institute.

Received: August 21, 2003
Revised: August 31, 2004
Accepted: September 30, 2004
Published: October 27, 2004

### References

Bassand, P., Bernard, A., Rafiki, A., Gayet, D., and Khrestchatisky, M. (1999). Differential interaction of the tSXV motifs of the NR1 and NR2A NMDA receptor subunits with PSD-95 and SAP97. Eur. J. Neurosci. *11*, 2031–2043.

Beattie, E.C., Carroll, R.C., Yu, X., Morishita, W., Yasuda, H., von Zastrow, M., and Malenka, R.C. (2000). Regulation of AMPA receptor endocytosis by a signaling mechanism shared with LTD. Nat. Neurosci. *3*, 1291–1300.

Brummelkamp, T.R., Bernards, R., and Agami, R. (2002). A system for stable expression of short interfering RNAs in mammalian cells. Science *296*, 550–553.

Cai, C., Coleman, S.K., Niemi, K., and Keinanen, K. (2002). Selective binding of synapse-associated protein 97 to GluR-A alpha-amino-5-hydroxy-3-methyl-4-isoxazole propionate receptor subunit is determined by a novel sequence motif. J. Biol. Chem. *277*, 31484–31490.

Carroll, R.C., Beattie, E.C., von Zastrow, M., and Malenka, R.C. (2001). Role of AMPA receptor endocytosis in synaptic plasticity. Nat. Rev. Neurosci. *2*, 315–324.

Chen, L., Chetkovich, D.M., Petralia, R.S., Sweeney, N.T., Kawasaki, Y., Wenthold, R.J., Bredt, D.S., and Nicoll, R.A. (2000). Stargazin regulates synaptic targeting of AMPA receptors by two distinct mechanisms. Nature *408*, 936–943.

Cho, K.O., Hunt, C.A., and Kennedy, M.B. (1992). The rat brain postsynaptic density fraction contains a homolog of the *Drosophila* discs-large tumor suppressor protein. Neuron *9*, 929–942.

Doerks, T., Bork, P., Kamberov, E., Makarova, O., Muecke, S., and Margolis, B. (2000). L27, a novel heterodimerization domain in receptor targeting proteins Lin-2 and Lin-7. Trends Biochem. Sci. *25*, 317–318.

Ehlers, M.D. (2000). Reinsertion or degradation of AMPA receptors determined by activity-dependent endocytic sorting. Neuron *28*, 511–525.

Ehrlich, I., and Malinow, R. (2004). Postsynaptic density 95 controls AMPA receptor incorporation during long-term potentiation and experience-driven synaptic plasticity. J. Neurosci. *24*, 916–927.

El-Husseini, A.E., Schnell, E., Chetkovich, D.M., Nicoll, R.A., and Bredt, D.S. (2000). PSD-95 involvement in maturation of excitatory synapses. Science *290*, 1364–1368.

El-Husseini, Ael-D., Schnell, E., Dakoji, S., Sweeney, N., Zhou, Q., Prange, O., Gauthier-Campbell, C., Aguilera-Moreno, A., Nicoll, R.A., and Bredt, D.S. (2002). Synaptic strength regulated by palmitate cycling on PSD-95. Cell *108*, 849–863.

Frank, J., Radermacher, M., Penczek, P., Zhu, J., Li, Y., Ladjadj, M., and Leith, A. (1996). SPIDER and WEB: processing and visualization of images in 3D electron microscopy and related fields. J. Struct. Biol. *116*, 190–199.

Gardoni, F., Mauceri, D., Fiorentini, C., Bellone, C., Missale, C., Cattabeni, F., and Di Luca, M. (2003). CaMKII-dependent phosphorylation regulates SAP97/NR2A interaction. J. Biol. Chem. *278*, 44745–44752.

Hayashi, Y., Shi, S.H., Esteban, J.A., Piccini, A., Poncer, J.C., and Malinow, R. (2000). Driving AMPA receptors into synapses by LTP and CaMKII: requirement for GluR1 and PDZ domain interaction. Science *287*, 2262–2267.

Hung, A.Y., and Sheng, M. (2002). PDZ domains: structural modules for protein complex assembly. J. Biol. Chem. *277*, 5699–5702.

Husi, H., Ward, M.A., Choudhary, J.S., Blackstock, W.P., and Grant, S.G. (2000). Proteomic analysis of NMDA receptor-adhesion protein signaling complexes. Nat. Neurosci. *3*, 661–669.

Jiang, Y., Lee, A., Chen, J., Ruta, V., Cadene, M., Chait, B.T., and MacKinnon, R. (2003). X-ray structure of a voltage-dependent K+ channel. Nature *423*, 33–41.

Karnak, D., Lee, S., and Margolis, B. (2002). Identification of multiple binding partners for the amino-terminal domain of synapse-associated protein 97. J. Biol. Chem. *277*, 46730–46735.

Kim, E., Niethammer, M., Rothschild, A., Jan, Y.N., and Sheng, M. (1995). Clustering of Shaker-type K+ channels by interaction with a family of membrane-associated guanylate kinases. Nature *378*, 85–88.

Kim, E., Cho, K.O., Rothschild, A., and Sheng, M. (1996). Heteromultimerization and NMDA receptor-clustering activity of Chapsyn-110, a member of the PSD-95 family of proteins. Neuron *17*, 103–113.

Kistner, U., Wenzel, B.M., Veh, R.W., Cases-Langhoff, C., Garner, A.M., Appeltauer, U., Voss, B., Gundelfinger, E.D., and Garner, C.C. (1993). SAP90, a rat presynaptic protein related to the product of the Drosophila tumor suppressor gene dlg-A. J. Biol. Chem. *268*, 4580–4583.

Leonard, A.S., Davare, M.A., Horne, M.C., Garner, C.C., and Hell, J.W. (1998). SAP97 is associated with the alpha-amino-3-hydroxy-5-methylisoxazole-4-propionic acid receptor GluR1 subunit. J. Biol. Chem. *273*, 19518–19524.

Lin, J.W., Ju, W., Foster, K., Lee, S.H., Ahmadian, G., Wyszynski, M., Wang, Y.T., and Sheng, M. (2000). Distinct molecular mechanisms and divergent endocytotic pathways of AMPA receptor internalization. Nat. Neurosci. *3*, 1282–1290.

Lois, C., Hong, E.J., Pease, S., Brown, E.J., and Baltimore, D. (2002). Germline transmission and tissue-specific expression of transgenes delivered by lentiviral vectors. Science *295*, 868–872.

Marfatia, S.M., Byron, O., Campbell, G., Liu, S.C., and Chishti, A.H. (2000). Human homologue of the Drosophila discs large tumor suppressor protein forms an oligomer in solution. Identification of the self-association site. J. Biol. Chem. *275*, 13759–13770.

Mauceri, D., Cattabeni, F., Di Luca, M., and Gardoni, F. (2004). Calcium/calmodulin-dependent protein kinase II phosphorylation drives synapse-associated protein 97 into spines. J. Biol. Chem. *279*, 23813–23821.

McGee, A.W., and Bredt, D.S. (1999). Identification of an intramolecular interaction between the SH3 and guanylate kinase domains of PSD-95. J. Biol. Chem. *274*, 17431–17436.

McGee, A.W., Dakoji, S.R., Olsen, O., Bredt, D.S., Lim, W.A., and Prehoda, K.E. (2001). Structure of the SH3-guanylate kinase module from PSD-95 suggests a mechanism for regulated assembly of MAGUK scaffolding proteins. Mol. Cell *8*, 1291–1301.

Migaud, M., Charlesworth, P., Dempster, M., Webster, L.C., Watabe, A.M., Makhinson, M., He, Y., Ramsay, M.F., Morris, R.G., Morrison, J.H., et al. (1998). Enhanced long-term potentiation and impaired learning in mice with mutant postsynaptic density-95 protein. Nature *396*, 433–439.

Nagai, T., Ibata, K., Park, E.S., Kubota, M., Mikoshiba, K., and Miyawaki, A. (2002). A variant of yellow fluorescent protein with fast and efficient maturation for cell-biological applications. Nat. Biotechnol. *20*, 87–90.

Niethammer, M., Kim, E., and Sheng, M. (1996). Interaction between the C terminus of NMDA receptor subunits and multiple members of the PSD-95 family of membrane-associated guanylate kinases. J. Neurosci. *16*, 2157–2163.

Ohi, M., Li, Y., Cheng, Y., and Walz, T. (2004). Negative staining and image classification – powerful tools in modern electron microscopy. Biol. Proced. Online *6*, 23–34.

Okabe, S., Urushido, T., Konno, D., Okado, H., and Sobue, K. (2001). Rapid redistribution of the postsynaptic density protein PSD-Zip45 (Homer 1c) and its differential regulation by NMDA receptors and calcium channels. J. Neurosci. *21*, 9561–9571.

Okamoto, K.-I., Nagai, T., Miyawaki, A., and Hayashi, Y. (2004). Rapid and persistent modulation of actin dynamics regulates postsynaptic reorganization underlying bidirectional plasticity. Nat. Neurosci. *7*, 1104–1112.

Park, S.H., Zarrinpar, A., and Lim, W.A. (2003). Rewiring MAP kinase pathways using alternative scaffold assembly mechanisms. Science *299*, 1061–1064.

Passafaro, M., Sala, C., Niethammer, M., and Sheng, M. (1999). Microtubule binding by CRIPT and its potential role in the synaptic clustering of PSD-95. Nat. Neurosci. *2*, 1063–1069.

Passafaro, M., Piech, V., and Sheng, M. (2001). Subunit-specific temporal and spatial patterns of AMPA receptor exocytosis in hippocampal neurons. Nat. Neurosci. *4*, 917–926.

Peng, J., Kim, M.J., Cheng, D., Duong, D.M., Gygi, S.P., and Sheng, M. (2004). Semi-quantitative proteomic analysis of rat forebrain postsynaptic density fractions by mass spectrometry. J. Biol. Chem. *279*, 21003–21011.

Philo, J.S. (1997). An improved function for fitting sedimentation velocity data for low-molecular-weight solutes. Biophys. J. *72*, 435–444.

Roh, M.H., Makarova, O., Liu, C.J., Shin, K., Lee, S., Laurinec, S., Goyal, M., Wiggins, R., and Margolis, B. (2002). The Maguk protein, Pals1, functions as an adapter, linking mammalian homologues of Crumbs and Discs Lost. J. Cell Biol. *157*, 161–172.

Rubinson, D.A., Dillon, C.P., Kwiatkowski, A.V., Sievers, C., Yang,

L., Kopinja, J., Rooney, D.L., Ihrig, M.M., McManus, M.T., Gertler, F.B., et al. (2003). A lentivirus-based system to functionally silence genes in primary mammalian cells, stem cells and transgenic mice by RNA interference. Nat. Genet. *33*, 401–406.

Rumbaugh, G., Sia, G.M., Garner, C.C., and Huganir, R.L. (2003). Synapse-associated protein-97 isoform-specific regulation of surface AMPA receptors and synaptic function in cultured neurons. J. Neurosci. *23*, 4567–4576.

Safferling, M., Tichelaar, W., Kummerle, G., Jouppila, A., Kuusinen, A., Keinanen, K., and Madden, D.R. (2001). First images of a glutamate receptor ion channel: oligomeric state and molecular dimensions of GluRB homomers. Biochemistry *40*, 13948–13953.

Sala, C., Futai, K., Yamamoto, K., Worley, P.F., Hayashi, Y., and Sheng, M. (2003). Inhibition of dendritic spine morphogenesis and synaptic transmission by activity-inducible protein Homer1a. J. Neurosci. *23*, 6327–6337.

Sans, N., Racca, C., Petralia, R.S., Wang, Y.X., McCallum, J., and Wenthold, R.J. (2001). Synapse-associated protein 97 selectively associates with a subset of AMPA receptors early in their biosynthetic pathway. J. Neurosci. *21*, 7506–7516.

Schnell, E., Sizemore, M., Karimzadegan, S., Chen, L., Bredt, D.S., and Nicoll, R.A. (2002). Direct interactions between PSD-95 and stargazin control synaptic AMPA receptor number. Proc. Natl. Acad. Sci. USA *99*, 13902–13907.

Sheng, M., and Kim, M.J. (2002). Postsynaptic signaling and plasticity mechanisms. Science *298*, 776–780.

Shi, S.H., Hayashi, Y., Petralia, R.S., Zaman, S.H., Wenthold, R.J., Svoboda, K., and Malinow, R. (1999). Rapid spine delivery and redistribution of AMPA receptors after synaptic NMDA receptor activation. Science *284*, 1811–1816.

Shin, H., Hsueh, Y.P., Yang, F.C., Kim, E., and Sheng, M. (2000). An intramolecular interaction between Src homology 3 domain and guanylate kinase-like domain required for channel clustering by postsynaptic density-95/SAP90. J. Neurosci. *20*, 3580–3587.

Siegel, L.M., and Monty, K.J. (1966). Determination of molecular weights and frictional ratios of proteins in impure systems by use of gel filtration and density gradient centrifugation. Application to crude preparations of sulfite and hydroxylamine reductases. Biochim. Biophys. Acta *112*, 346–362.

Sokolova, O., Kolmakova-Partensky, L., and Grigorieff, N. (2001). Three-dimensional structure of a voltage-gated potassium channel at 2.5 nm resolution. Structure (Camb) *9*, 215–220.

Songyang, Z., Fanning, A.S., Fu, C., Xu, J., Marfatia, S.M., Chishti, A.H., Crompton, A., Chan, A.C., Anderson, J.M., and Cantley, L.C. (1997). Recognition of unique carboxyl-terminal motifs by distinct PDZ domains. Science *275*, 73–77.

Sprengel, R., Suchanek, B., Amico, C., Brusa, R., Burnashev, N., Rozov, A., Hvalby, O., Jensen, V., Paulsen, O., Andersen, P., et al. (1998). Importance of the intracellular domain of NR2 subunits for NMDA receptor function in vivo. Cell *92*, 279–289.

Srivastava, S., Osten, P., Vilim, F.S., Khatri, L., Inman, G., States, B., Daly, C., DeSouza, S., Abagyan, R., Valtschanoff, J.G., et al. (1998). Novel anchorage of GluR2/3 to the postsynaptic density by the AMPA receptor-binding protein ABP. Neuron *21*, 581–591.

Stein, V., House, D.R., Bredt, D.S., and Nicoll, R.A. (2003). Postsynaptic density-95 mimics and occludes hippocampal long-term potentiation and enhances long-term depression. J. Neurosci. *23*, 5503–5506.

Tavares, G.A., Panepucci, E.H., and Brunger, A.T. (2001). Structural characterization of the intramolecular interaction between the SH3 and guanylate kinase domains of PSD-95. Mol. Cell *8*, 1313–1325.

Tiffany, A.M., Manganas, L.N., Kim, E., Hsueh, Y.P., Sheng, M., and Trimmer, J.S. (2000). PSD-95 and SAP97 exhibit distinct mechanisms for regulating K(+) channel surface expression and clustering. J. Cell Biol. *148*, 147–158.

Tomita, S., Chen, L., Kawasaki, Y., Petralia, R.S., Wenthold, R.J., Nicoll, R.A., and Bredt, D.S. (2003). Functional studies and distribution define a family of transmembrane AMPA receptor regulatory proteins. J. Cell Biol. *161*, 805–816.

Walikonis, R.S., Jensen, O.N., Mann, M., Provance, D.W., Jr., Mercer, J.A., and Kennedy, M.B. (2000). Identification of proteins in the postsynaptic density fraction by mass spectrometry. J. Neurosci. *20*, 4069–4080.

Wu, H., Reissner, C., Kuhlendahl, S., Coblentz, B., Reuver, S., Kindler, S., Gundelfinger, E.D., and Garner, C.C. (2000). Intramolecular interactions regulate SAP97 binding to GKAP. EMBO J. *19*, 5740–5751.

Wu, H., Nash, J.E., Zamorano, P., and Garner, C.C. (2002). Interaction of SAP97 with minus-end-directed actin motor myosin VI. Implications for AMPA receptor trafficking. J. Biol. Chem. *277*, 30928–30934.